DETERMINATION OF TRUE STRESS-STRAIN CURVE FOR ISOTROPIC MATERIALS WITH THIN SHEET TENSILE SPECIMENS

Yoshihiro Lima Nemoto, M.Eng.
Depto. Engenharia Mecânica - Universidade Federal de Santa Catarina
CP 476, Florianópolis – SC, 88040-900
nemoto@grante.ufsc.br

Paulo de Tarso R. Mendonça, Ph.D.
Depto. Engenharia Mecânica - Universidade Federal de Santa Catarina
CP 476, Florianópolis – SC, 88040-900
mendonca@grante.ufsc.br

Edison da Rosa, Dr.Eng.
Depto. Engenharia Mecânica - Universidade Federal de Santa Catarina
CP 476, Florianópolis – SC, 88040-900
darosa@emc.ufsc.br

Abstract. *Determination of the true stress-strain curve for a material available in the form of bars or thick plates can be done in two ways. If the interest is in obtaining data until the development of the necking, engineering stress and strain are recorded and corrected by using the incompressible condition of uniform plastic flow developed in the specimen. If the interest resides in data after necking, the inhomogeneous deformation makes it necessary record load and diameter reduction of the specimen. A correction for the true stress for necking is then obtained by using the Bridgman equation.*

In design of parts made of thin plates or sheets, use of material data obtained from round tensile specimens is not always adequate, since, either the material is produced only in form of sheet, or shows different properties in its sheet or bar forms due to differences in fabrication processes. Until recently there was no consistent method to determine true stress-strain curve for a material by rectangular cross-section tensile specimens. The main challenge in a experimental procedure is that diffuse necking makes the cross section no longer rectangular, rendering almost impossible to measure its dimensions in real time.

This paper reviews the findings of Z.L. Zhang, who showed that the area reduction could be normalized by the uniaxial strain at maximum load and the aspect ratio. A finite element three-dimensional analysis on the diffuse necking behavior is performed to develop a simple procedure to obtain the area reduction evolution in terms of measurements of the load-thickness reduction curve, which is then used to construct the true stress-logarithmic strain curve. Three different materials were tested in laboratory, and the accuracy of the formulation is shown to be good.

Keywords *True stress-strain curve, isotropic materials, sheet tensile specimen, plastic deformation.*

1. Introduction

Knowledge of the true stress-strain curve of a material is necessary in applications involving large deformations, for example, in the metal forming analysis or in ductile fracture analysis of parts. When it is possible to construct round tensile specimens, two situations may arise. First, if the interest is obtaining the material data until the development of the necking, a simple experimental procedure is possible, consisting in measuring and recording engineering stress and strain (ABNT, NBR-6152, 1980). True stresses and logarithmic stains are next obtained correcting the data using the incompressible condition of uniform plastic flow that develops in the specimen (Dieter, 1986). Second, if the interest resides in data after necking, the inhomogeneous deformation makes it necessary recording load and diameter reduction of the specimen. The true stress is next corrected by using the Bridgman equation.

When analyzing parts fabricated from sheets, an ideal procedure would be using material data obtained directly from rectangular cross section specimens. However, it is not always possible to machine tool round specimens from a thin sheet, which can be easily seen comparing standard diameters for round specimens, of 8 millimeters, with usual sheet thickness of 2 millimeters or less. Nevertheless, until recently, there was no consistent experimental method to determine true stress-strain curve for a material by rectangular cross-section tensile specimens.

The most difficult part of experimental procedure is to measure the cross section dimensions, because after diffuse necking takes place, the cross section changes its original rectangular format, compromising the necessary accuracy to describe the cross section area change. In a ductile rate-independent material, plastic instability, the necking begins just after the maximum load, in a similar way as the neck of a round specimen. The deformation continues diffuse around a certain extent of the specimen, under falling load, until the development of a localized neck. The range of deformation of localized neck is usually short and the process is very short before fracture.

This paper reviews the findings of Zhang *et al*. (1999), who showed that the area reduction during diffuse necking phase could be decomposed in two parts, the proportional area reduction and a non-proportional area reduction associated with the shape change of the section.

A finite element three-dimensional analysis on the diffuse necking behavior is performed and showed that the non-proportional area reduction could be approximately normalized by the uniaxial strain at maximum load and the cross section aspect ratio. This normalization allows the development of a simple procedure to obtain the area reduction evolution in terms of measurements of the thickness in the center of the cross section, which is relatively easy to perform, and the load history, which allows the determination of true strain and average true stress. An additional difficulty arises from the observation of Aronofsky, (1951), that stresses are not uniformly distributed along the rectangular cross section after necking, making necessary a correction of the average true stress before it can be used as uniaxial material flow stress. It is shown that the Bridgman equation can be applied for rectangular cross section in the same way it is used for circular ones.

In the following, the numerical procedure described by Zhang is reviewed and implemented. Three different materials were tested in laboratory, using rectangular and round cross section specimens. Materials with different characteristics of those tested by Zhang were chosen to estimate the range of applicability of the formulation. The materials tested were: stainless steel 316, aluminum 6351, cooper CA110 and cooper CA122. Combining the present results with those obtained from the materials tested by Zhang, the method seems reliable to determine true stress-strain curves until about 50% of thickness deformation, which can represent until about 100% deformation depending on the cross section aspect ratio.

2. Area deformation

It is well known that deformation just after the maximum load marks the beginning of necking. The condition of constant volume of plastic deformation allows the Hencky deformation to be expressed as $\varepsilon = \ln\left(A_o / A\right)$, where A and A_o are the current and initial cross-section areas, respectively. For round specimens of isotropic materials, the cross section remains circular in the entire range of deformations until fracture. Thus, the area changes are obtained directly by diameter measurements. In case of rectangular cross section, however, after the onset of necking, the section becomes distorted, assuming a shape similar to that depicted in Fig. 1. The exact measurement of the area evolution, in general, is beyond the capabilities of regular material testing laboratories in industrial and educational institutions. A usual mean to circumvent the problem (ASTM, E-8M, 1997) consists in approximate the thickness variation by a polynomial function of second degree, measure the thickness in three different positions, as indicated in Fig.1b, and evaluate the effective thickness by $t_e = \left(t_1 + 4t_2 + t_3\right)/6$. A similar procedure is used with the width of the minimum section, and the effective area is estimated. Numerical simulations shown below indicate that a correct evaluation of the profile is essential for an accurate computation of area and, as a consequence, of the true stresses and strains.

One of the goals of the procedure discussed in this paper is the possibility of obtaining a good area estimate taking with measurements of a single parameter, the thickness t_2 at the center of the cross section. First, it is assumed that deformation can be decomposed in proportional and non-proportional parts. In the formed one, the section keeps its rectangular form, Fig. 1a, similarly to what happens in the circular section. The non-proportional deformation accounts for the shape distortion, as in Fig. 1b.

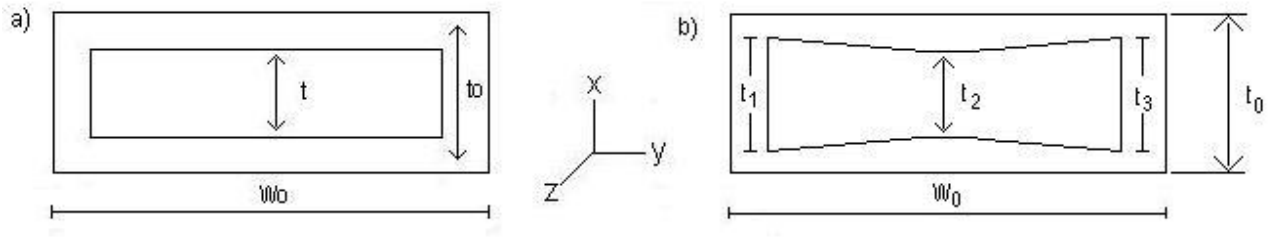

Figure 1. (a) Proportional deformation in round and rectangular cross sections. (b) Non-proportional of rectangular cross section.

Considering A, A_o, A_p and A_{np} as the current cross-section area, original, proportional and non-proportional areas, respectively, one can define the total, proportional and non-proportional area changes as $\Delta A = A_o - A_p$, $\Delta A_p = A_o - A_p$ and $\Delta A_{np} = A - A_p$, respectively. In case the bar is loaded in tension, all three area changes must be non-negative. Prior to the maximum load, one must have $\Delta A_{np} = 0$, due to the hipothesis of homogeneous deformation.

An expression for the proportional part of deformation in the rectangular cross section can be derived. Assuming $\varepsilon_x = \varepsilon_y$, there is a proportionality constant *a* such that $W_o = a\,t_o$ and $W = a\,t$, where *W, t* etc. are the cross section dimensions as shown in Fig. 1a. The original and actual areas are $A_o = W_o\,t_o$. and $A = W\,t$. Thus, $A_o = W_o t_o = a\,t_o^2$ and $A = Wt = a\,t^2$. Using $t = t_o - \Delta t$, the proportional area variation is $\Delta A_p = a(2t_o\Delta t - \Delta t^2)$, and

$$\left(\frac{\Delta A}{A_o}\right)_p = \frac{2\Delta t}{t_o} - \left(\frac{\Delta t}{t_o}\right)^2 \tag{1}$$

3. Finite element analysis

The entire flow process undertaken by a rectangular specimen in tension test was modeled by finite element method. Figure 2 shows the region modeled, mesh, and dimensions *C, L* and t_o of the model. Cross-section aspect ratios $RF \equiv L/t_o = 2,3,4,5$ and 8 have been analyzed. Following Zhang *et al*, the initial length is fixed as $C = 24t_o$, except for *RF* = 8, when $C = 40t_o$. The thickness is t_o =1.5 mm in all cases.

The analysis was performed using Ansys 7.0 with large deformation and rate-independent incremental plasticity, with multi-linear isotropic material hardening and von Mises yield criteria. Following the incremental solution from the origin of the graph load x displacement, the stiffness of the bar decreases gradually until the point of maximum load, when the stiffness matrix becomes singular. This phenomenon leads to the use of the arc-length method in the analysis.

The element used is the 20 nodes solid brick, which is able to withstand the mesh distortion observed during plastic flow. The mesh configuration was determined from a mesh sensitivity analysis, observing responses of maximum load, thickness at specimen center at maximum load and load at 50% thickness reduction; in all cases, model with aspect ratio 4 was used. The results in Fig. 3a show maximum loads almost insensitive to mesh sizes above 3520 nodes. The thickness at maximum load, Fig. 3b also shows a ratio standard deviation/average value of only 0,44%, if the mesh with 7865 nodes is discarded. The results of load at 50% thickness reduction in Fig. 4a indicate the adequacy of meshes with more than 2620 nodes.

As a result, a mesh 2620 nodes was adopted in the analysis. In order to localize the neck, a small notch is applied at the center of the specimen. The imperfection is cut along the thickness, at both sides, with depth of 0.004*L* and radius $12\,t_o$. We observe that larger notches can affect the numerical results, (also Tvergaard, 1991), and smaller ones are more difficult to be machined on the specimens. The presence of the notch defines a division of the mesh in two regions, one more refined in the vicinity of notch, with 7 elements in the axial direction (Fig.2). The region is modeled by 8 elements of progressively changing lengths. The meshes along the width and thickness directions are uniform, with 10 and 3 elements, respectively.

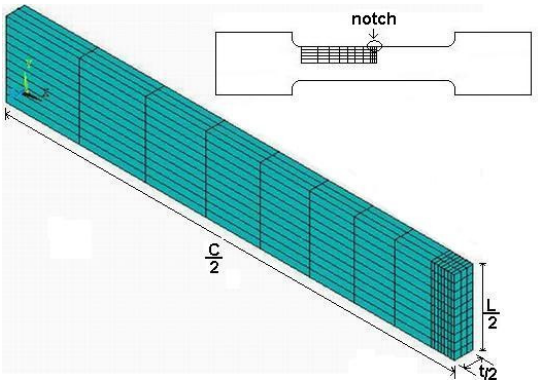

Figure 2. Finite element mesh of of 1/8th of the specimen, with refinement around the notch.

The non-linear method of solution used is displacement-controlled due to instability of the specimen at the maximum load point. A reference tensile load is applied to the specimen, and load factors are determined, together with nodal displacement solutions, along the equilibrium path, according the arc-length method (Owen, 1997). The choice of these values has influence on processing time, as shown in Fig. 4b. Based on these results, the numerical experiments were conducted with arc-length factor *f* = 4 and the reference load F_r=2 kN With these parameters and the mesh of 2620 nodes, a simulation takes about 15 minutes on a personal computer with 1500Mb of RAM and 2000Mz clock.

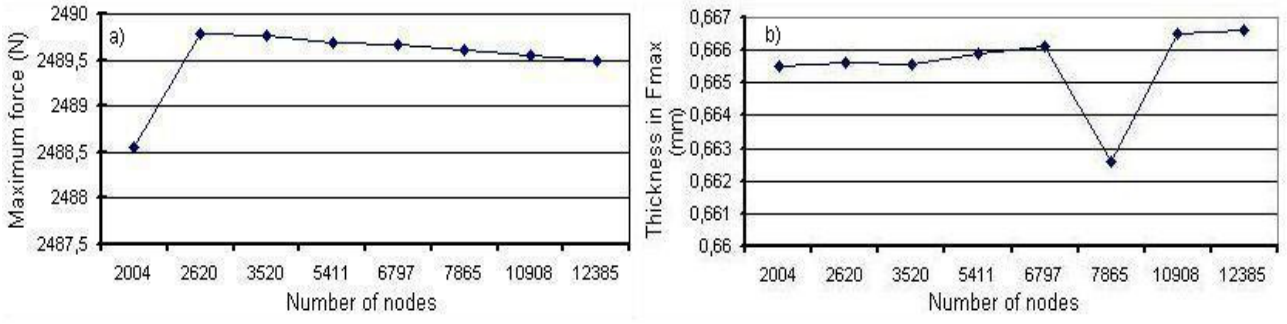

Figure 3. (a) Maximum load. (b) Thickness at the maximum load point.

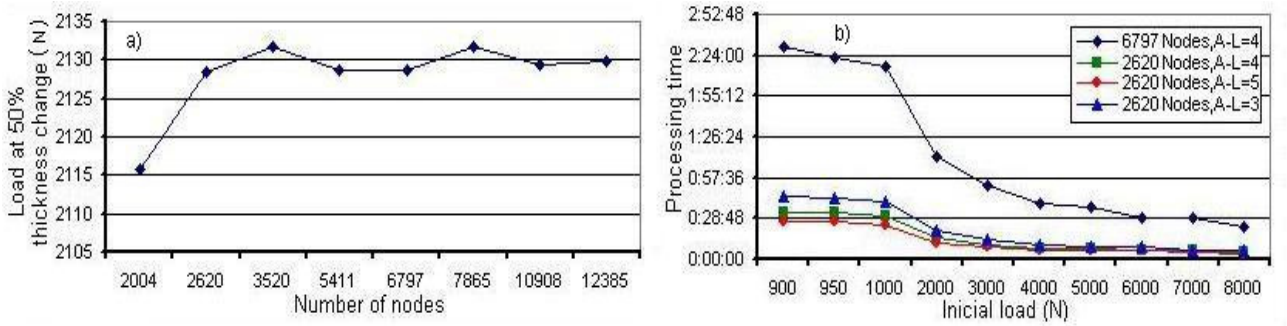

Figure 4. (a) load at 50% thickness reduction for different mesh refinements. (b) Processing time.

The numerical analysis were based on materials with isotropic hardening behavior, whose rate independent flow curve is described by the following variation of the Ramberg-Osgood equation:

$$\bar{\sigma} = \sigma_o \left(1 + \frac{\bar{\varepsilon}_p}{\varepsilon_o} \right)^n \tag{2}$$

where $\bar{\sigma}$ and $\bar{\varepsilon}_p$ are real flow stress and real equivalent plastic strain, σ_o and ε_o are stress and strain parameters and n is the hardening exponent. Following Zhang, we fixed the values of elastic modulus E and Poisson coefficient to be $E/\sigma_o = 500$ and $\nu = 0.3$. However, as it will be seen, expeimental results seems to indicate that the validity of the developed model is not restricted to this range of material properties. The only material parameter changed in the numerical models was the hardening exponent, which took the values $n = 0.05$, 0.10, 0.15 and 0.20. It is worth noting that this range covers most of the types of steel, from low to high carbon content, and that n is about 0.5 in cooper and brass (following typical values from Dieter, 1986, for instance). The material data were applied to the program in the form of a multilinear curve.

4. Relation area change versus thickness change

Finite element analyses were performed in 20 models (five aspect ratios RF = 2,3,4,5 and 8 and $n = 0.05$, 0.10, 0.15 and 0.20). In each case, the total area change ΔA and thickness change at the center of the specimen, Δt, were computed. The values of the area change showed to be very sensitive to the accuracy of the procedure used in its computation. The current area A is obtained adding the deformed areas of the element faces common to the cross-section of the model. The element used has 8 nodes on the surface. The simple attempt of subdividing the element in triangles defined by the nodes, lead to crude results. This, in turn, generated large negative non-proportional area changes prior to the maxium load. Therefore, all results shown in this paper were obtained by a separate post-processing based on a consistent integration of the current area of the element, using nodal displacements, nodal coordinates and the original bi-qudratic shape-functions of the element.

For each numerical model, a plot load versus $\Delta t / t_o$ and $\left(\Delta A_{np} / A_o \right) \times \Delta t / t_o$ are computed. Figures 5a and 5b show brute results for stainless steel and cooper. These results are to be processed using the model described next. Zhang et al, using numerical simulation similar to the one described in section 3 of this paper, generated curves

$\left(\Delta A_{np} / A_o\right) \times \Delta t / t_o$ for different hardening constant *n* and aspect ratios RF. Figure 6b shows part of the results obtained in this way, for RF=4. The similarity between the curves for different RF allows then to be normalized by dividing each curve by value of the non-proportional area change at the thickness change $\Delta t / t_o = 0.5$, i.e., $\left(\Delta A_{np} / A_o\right)_{\Delta t / t_o = 0.5}$. It is seen in Fig. 6c that all normalized curves show reasonable coincidence for $\Delta t / t_o \le 0.5$. For materials with different *n* the behavior is similar.

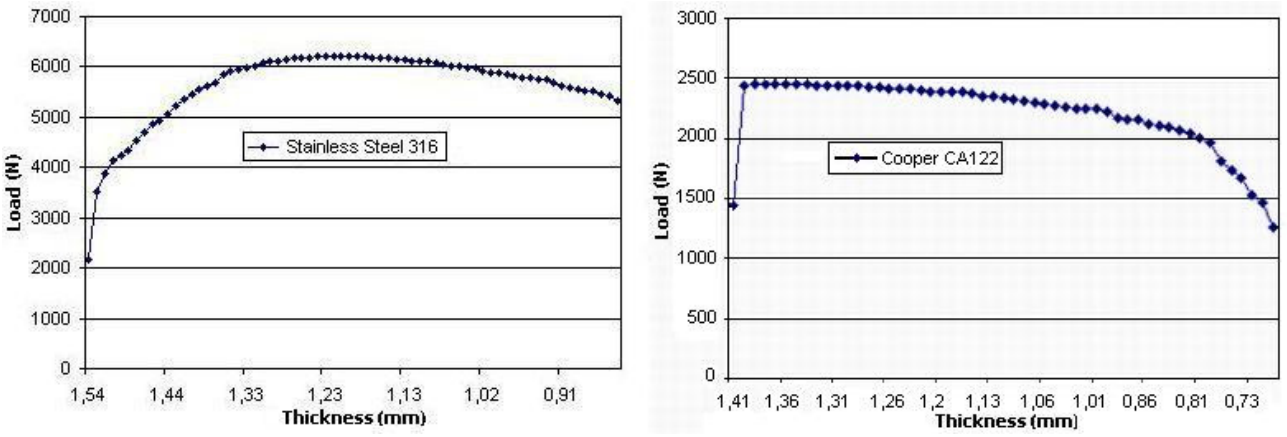

Figure 5. (a) Brute results for stainless steel. (b) brute results for cooper CA122.

The values of $\left(\Delta A_{np} / A_o\right)_{\Delta t / t_o = 0.5}$ used to normalize the data have been collected and displayed in the graph of Fig.7a for all different aspect ratios RF and n. Again, the curves are all similar in shape, and can be normalized by dividing each one by its value at some chosen value of RF. Thus, normalizing by the value at RF = 4, the four curves almost coincide, as shown in Fig.7b. A curve fit gives an equation similar to the one by Zhang et al ($f_{RF}(RF) \simeq 0.1686 + 0.6 \ln RF$):

$$f_{RF}(RF) \equiv \frac{\Delta A_{np} / A_o}{\left(\Delta A_{np} / A_o\right)_{\Delta t / t_o = 0.5, RF = 4}} \simeq 0.1994 + 0.5831 \ln RF \tag{3}$$

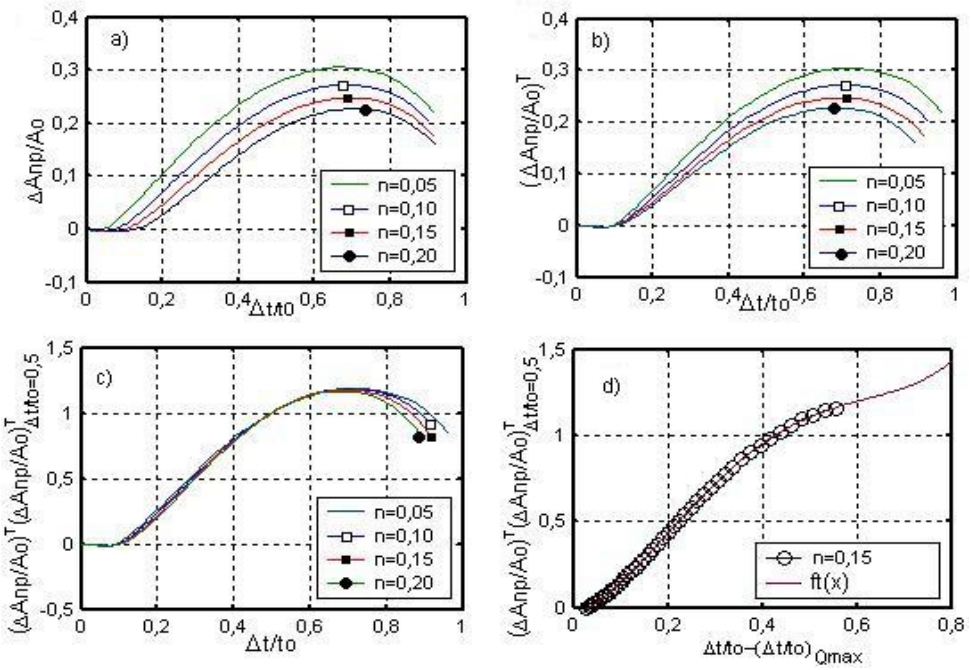

Figure 6. Normalizing procedure curves for RF=4 specimens.

A different reorganization of the computed data can be done to obtain a graph like the one in Fig. 6a, showing $\left(\Delta A_{np}/A_o\right)\times\Delta t/t_o$ for different *n,* in a fixed aspect ratio RF = 4. It is seen that every curve begins with a plateau, which ends at different thickness variation, each end associated with the corresponding maximum load. The parts of each curve beyond the plateau are similar, which suggests a correction by a shift in the $\Delta t/t_o$ axis. Therefore, a shift D_t the *x*-axis is applied such that

$$\frac{\Delta t}{t_o} \rightarrow \frac{\Delta t}{t_o} - D_t \qquad \text{where} \qquad D_t = \left(\frac{\Delta t}{t_o}\right)_{n,\,F_{\max}} - \left(\frac{\Delta t}{t_o}\right)_{n=0.15,\,F_{\max}} \tag{4}$$

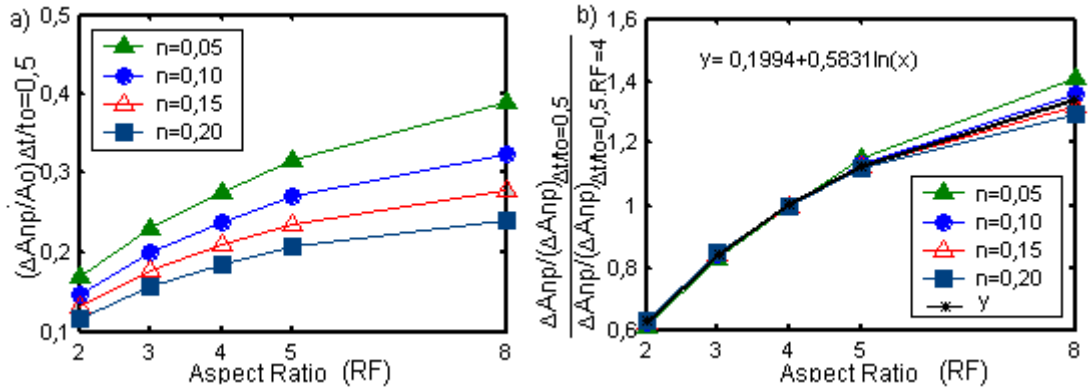

Figure 7. (a) The values of $\left(\Delta A_{np}/A_o\right)_{\Delta t/t_o=0.5}$ used to normalize the data. (b) Non-proportional area reduction curves due to the respective 50% thickness reduction specimens with aspect ratio RF=4.

In this way, all curves, except the one for n = 0.15, are shifted, such that all of the resulting $\left(\Delta A_{np}/A_o\right)^T\times\Delta t/t_o$ curves have the initial plateaus with the same length. The shifted curves, in turn, are similar in shape, and each one can be normalized by its value at $\Delta t/t_o = 0.5$. The resulting curves, $\left(\Delta A_{np}/A_o\right)^T/\left(\Delta A_{np}/A_o\right)^T_{\Delta t/t_o=0.5}\times\Delta t/t_o$, coincide almost perfectly until approximately $\Delta t/t_o = 0.6$. The part of curve beyond the plateau is obtained by a coordinate shift, as seen in Fig.6d. A curve fit results in

$$f_t(x) \equiv \frac{\left(\Delta A_{np}/A_o\right)^T}{\left(\Delta A_{np}/A_o\right)^T_{\Delta t/t_o=0.5}} \simeq c_o + c_1 x + c_2 x^2 + c_3 x^3 + c_4 x^4 \qquad \text{where} \quad x = \left(\frac{\Delta t}{t_o}\right) - \left(\frac{\Delta t}{t_o}\right)_{F_{\max}} \tag{5}$$

and $c_o = -0.04306$, $c_1 = 0.9912$, $c_2 = 11.249$, $c_3 = -24.818$ and $c_4 = 15.104$. These values are different of those obtained by Zhang et al (1999), but the resulting values of the function are similar in the range $0.01 < \left(\Delta t/t_o\right)_{F_{\max}} < 0.1$.

The values of $\left(\Delta A_{np}/A_o\right)_{\Delta t/t_o=0.5}$ necessary to normalize of the shifted curves $\left(\Delta A_{np}/A_o\right)^T\times\Delta t/t_o$ are obtained from figures like the 6b, for RF=4, collecting pairs $\left(n;\left(\Delta A_{np}/A_o\right)_{\Delta t/t_o=0.5}\right)$. But, since each curve *n* has its maximum load at a different $\left(\Delta t/t_o\right)_{F_{\max}}$, it is also possible to collect pairs $\left(\left(\Delta t/t_o\right)_{F_{\max}};\left(\Delta A_{np}/A_o\right)_{\Delta t/t_o=0.5}\right)$. From these sets of points, a curve fit gives the relation

$$f_m\left(\left(\frac{\Delta t}{t_o}\right)_{F_{\max}}\right) \equiv \left(\frac{\Delta A_{np}}{A_o}\right)_{\Delta t/t_o=0.5.} \simeq 0.2759 - 0.8643\left(\frac{\Delta t}{t_o}\right)_{F_{\max}} \qquad \text{and} \qquad n \simeq 0.002015 + 1.984\left(\frac{\Delta t}{t_o}\right)_{F_{\max}} \tag{6}$$

Both functions are valid for aspect ratio RF=4.

A detailed analysis of the results and relations breifly described above leads to the following equation for calculating the non-proportional area change for arbitrary *n* and RF:

$$\frac{\Delta A_{np}}{A_o} = f_{RF}(RF) f_t\left(\frac{\Delta t}{t_o} - \left(\frac{\Delta t}{t_o}\right)_{F_{\max}}\right) f_m\left(\left(\frac{\Delta t}{t_o}\right)_{F_{\max}}\right) \tag{7}$$

where f_{RF}, f_t and f_m are given in Eqs.(3), (5) and (6) respectively. Once this model has been verified, it is used as follow. The experimental data obtained from an unknown material generates a curve $F \times (\Delta t / t_o)$ such as Fig. 5a or 5b. From this curve, the value of $(\Delta t / t_o)$ at maximum load, $(\Delta t / t_o)_{F_{\max}}$, is determined, the curve $(\Delta A / A_o)_{np} \times (\Delta t / t_o)$ is obtained from Eq.(7) and the total area change $(\Delta A / A_o)_{np} \times (\Delta t / t_o)$ is computed from the proportional area change using Eq.(1). Next, a curve average true stress versus logarithmic strain, $\sigma_{av} \times \varepsilon$, is obtained by $\sigma_{av} = F / A$ and $\varepsilon = \ln(A_o / A)$. Finally, the correction to the stress at neck is done using the Bridgman equation, which, for round tensile specimens is

$$\sigma = \sigma_{av}\left[\left(1 + \frac{1R}{a}\right)\ln\left(1 + \frac{\sigma_{av}}{2R}\right)\right]^{-1} \tag{8}$$

where *a* is the current radius of the neck and *R* is the radius of curvature of the neck in the longitudinal plane of the specimen. An empirical expression for *a/R* is given by Le Roy et al, 1981 as $a / R = 1.1(\varepsilon - \varepsilon_{F_{\max}})$. Results obtained by this equation for rectangular specimens have also been reasonably good, and are used in the results of this paper.

5. Experimental results and conclusions

Three materials (stainless steel 316, aluminum 3105-H14 and cooper CA122) were tested using ectangular cross-section specimens, following the proposed area change model: for each material, the experimental data is treated by Eqs.(7) and (8) and the true stress-strain curve is estimated. Next, this curve is fed to the finite element model and the tensile test is simulated. The non-proportional area change and thickness change curves are numerically obtained. These data are in turn processed by Eqs. (7) and (8), and a second true stress-strain curve is obtained. Figure 7 show the experimental load x thickness curves for the stainless steel and cooper, and Fig. 8 show the stress-strain curves for the stainless steel and cooper. In each of the figures 8a, 8b and 9, three curves are shown: (1) the non-corrected curve, obtained from the area change model, Eq.(7); (2) a curve obtained by correcting the last curve by the Bridgman equation (8); (3) the experimental curve.

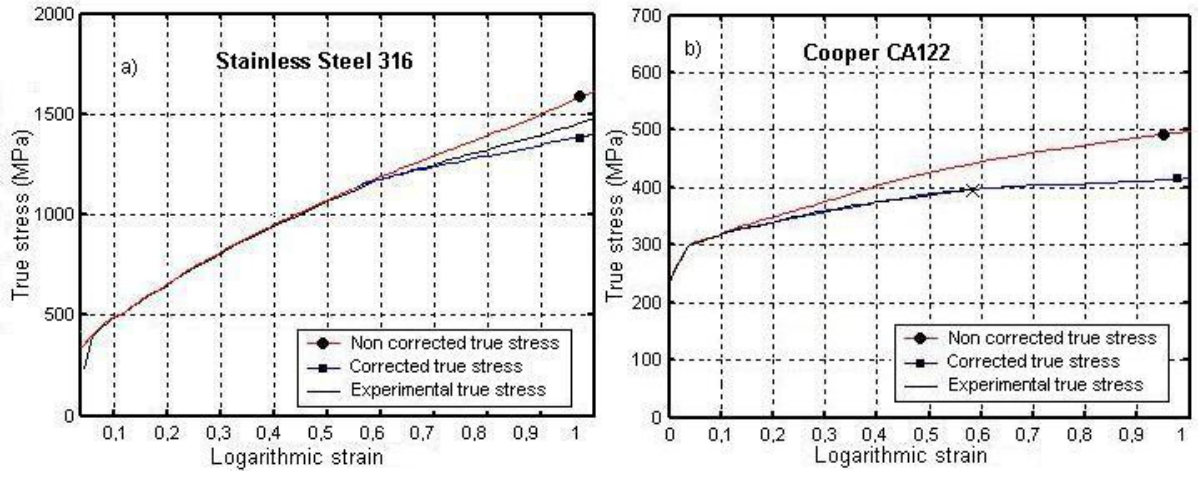

Figure 8. (a) True stress-strain curves for Stainless steel 316. (b) True stress-strain curves for Cooper CA122.

6. Conclusions

In all three materials tested, the true stress-strain curves obtained by the model correlates well with the experimental curve. Zhang et al performed similar comparisons, testing steel D and aluminum M3, and found equally good agreement. It is worth noting that none of these five materials reported can be modeled by the single parameter exponential equation (2), used to generate the area change model, yet the results are good in all cases. These suggest the possibility this method could be used for a larger range of materials.

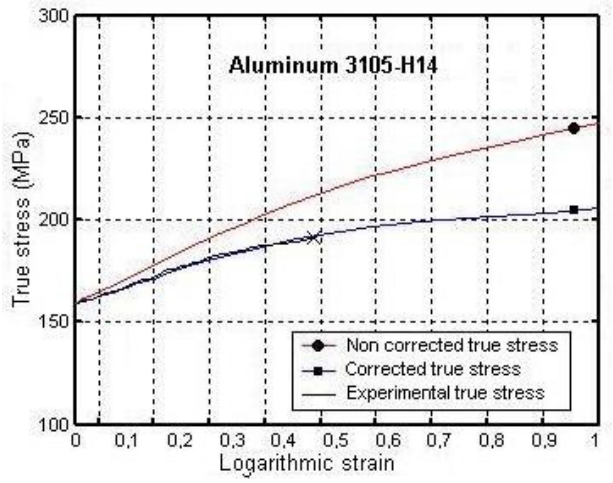

Figure 9. True stress-strain curves for Aluminum 3105-H14.

7. Acknowledgements

The authors would like to thank CNPq – Brasilian Council for Research and FINEP – National Financer for Resarch, for their financial support.

8. References

ABNT, NBR-6152, 1980 . "Materiais Metálicos - Determinação das propriedades mecânicas à tração".
ANSYS 7.0 Release, Helpdesk.
Aronofsky, J., 1951. "Evaluation of stress distribution in the symmetrical neck of flat tensile bars", Journal of Aplied Mechanics, vol.18, Dallas, U.S.
ASTM, A-370-77, 1977. "Mechanical testing of steel products".
ASTM, E-8M, 1997 . "Standart test methods for tension testing metallic materials [Metric] ".
Bathe, K.-J. 1982. "Finite element procedures in engineering analysis", Prentice-Hall, Inc., N.J., USA.
Chen, W.F., Han, D.J., 1988. "Plasticity for Structural Engineers", Springer-Verlag, New York, USA.
Cook, R.D., Malkus, D.S., Plesha, M.E., 1988. "Concepts and applications of finite element analysis", John Wiley & Sons, N.Y.
Dieter, G.E.Jr., 1986. "Mechanical Metallurgy", International student edition, MacGraw-Hill.
Hinton, E., Owen, D.R.J., 1980. "Finite elements in plasticity", Pineridge, Swansea,U.K.
Hughes, T.H., 1987. "The finite element method - linear static and dynamic finite element analysis", Prentice-Hall, Inc., N.J.
Knott, J.F., 1979. "Fundamentals of fracture mechanics", Butterworth,3rd ed., Norwich, UK.
Le Roy, G., Embury, J.D., Edward, G., Ashby, M.F., 1981. "A model of ductile fracture based on the nucleation and growth of voids", Acta Metallurgica, vol.29, p.1509 a 1522, Great Britain, U.K.
Malvern, E.L. 1969. "Introduction to the mechanics of a continuous medium", prentice-hall, Inc., N.J.
Neuber, H., 1961. Journal of Applied Mechanics, vol.28, p.544.
Owen, D.R.J., 1997. "Computation Plasticity: Small and Large Finite Element Analysis of Inelastic Solids". U.S.,Copyright.
Souza, S.A., 1982. "Ensaios mecânicos de materiais metálicos-fundamentos téoricos e práticos", Ed. Edgard Blucher LTDA., 5ª edição, São Paulo, Brasil.
Szabo, B., Babuska, I. 1991. "Finite element analysis", John Wiley & Sons, Inc., N.Y.
Tvergaard, V., 1991. "Necking in tensile bars with rectangular cross-section", Computer Methods in Applied Mechanics and Engineering, 103, 273-90.
Zhang, Z.L., Hauge, M., Odegard, J., Thaulow, C., 1999. "Determining material true stress-strain curve from tensile specimens with retangular cross section". International Journal of Solids and Structures, Trondheim, Norway.

9. Responsibility notice

The authors are the only responsible for the printed material included in this paper.